GENE-523-A161-1094
DRF 137-0010-06

Structural Evaluation and Justification of the Nine Mile Point 1 Core Shroud for Continued Operation

Performed By: _____
Betty J. Branlund
Senior Engineer
Structural Mechanics Projects

_____
Barry M. Gordon
Principal Engineer
BWR Technology

Approved By: _____
Sampath Ranganath, PhD
Manager, Engineering and Licensing
Consulting Services

GE Nuclear Energy
San Jose, CA

IMPORTANT NOTICE REGARDING CONTENTS OF THIS REPORT

Please Read Carefully

The only undertakings of the General Electric Company (GE) respecting information in this document are contained in the contract between Niagara Mohawk Power Company and GE, and nothing contained in this document shall be construed as changing the contract. The use of this information by anyone other than Niagara Mohawk Power Company or for any purpose other than that for which it is intended under such contract is not authorized; and with respect to any unauthorized use, GE makes no representation or warranty, and assumes no liability as to the completeness, accuracy, or usefulness of the information contained in this document, or that its use may not infringe privately owned rights.

Table of Contents

1. INTRODUCTION

This report presents the structural evaluation and justification for continued operation of the Nine Mile Point Unit 1 (NMP-1) plant until February of 1995. Recently, inspection of the Oyster Creek core shroud revealed significant indications at the mid-beltline weld, H4. Due to similarities between Oyster Creek and NMP-1, it is prudent to determine if similar cracking could be expected in NMP-1. It is also prudent to determine that if the Oyster Creek cracking were present in NMP-1, the cracking is structurally acceptable for operation until the planned outage in February of 1995. Inspection of the NMP-1 core shroud is planned for this next outage.

The structural justification for continued operation is presented in this reported as outlined in the following analyses:

1. Discussion of comparison of NMP-1 and Oyster Creek based on water chemistry, fluence and on-line years. This can be used as a basis to establish that any cracking in the NMP-1 core shroud is likely to be bounded by that observed in the Oyster Creek core shroud.

2. GE PLEDGE crack growth rate modeling to estimate a NMP-1 specific crack growth rate. This calculation will show that the estimated crack growth rate in the NMP-1 core shroud is less than 5×10^{-5} in/hr, which has been typically used for core shroud cracking.

3. Flaw evaluation using the Oyster Creek indications and considering crack growth during the current operating cycle until February of 1995.

Results of the comparison between NMP-1 and Oyster Creek show that the cracking in Oyster Creek is likely to bound that which may be expected in the NMP-1 shroud. In addition, the flaw evaluation and crack growth rate evaluation demonstrate that the structural integrity of the NMP-1 core shroud weld H4 is assured assuming that the same indications in the Oyster Creek H4 weld are present in the NMP-1 H4 weld.

2. DESCRIPTION OF INDICATIONS

The indications found in the Oyster Creek core shroud H4 weld are used in this structural evaluation. The results of the Oyster Creek H4 inspection are shown in Appendix A. These figures illustrate the indication depths at various azimuthal locations in the core shroud. At some locations, indications were found in both the ID and OD (In some cases one crack was above the weld and the other was below the weld). For this case, the indications were analyzed as a combined depth of the two flaws. For the areas which were not inspected, through-wall indications were assumed.

Figure 2-1 is a schematic showing the ligament configuration based on the Oyster Creek results. Figure 2-1 shows the ligament configuration after application of the proximity criteria; this configuration is used for calculating the limit load criteria. The following conservative assumption were used to determine the assumed indications:

1. Each indication was characterized by the maximum depth of the indication over the entire length of the indication.
2. A crack depth uncertainty factor of 0.3" was added to the depth of each crack.
3. An estimated crack growth until the next inspection with a crack growth rate of 5×10^{-5} in/hr was added to each crack depth.
4. At locations where indications were found on both the ID and OD, the depth was assumed to be the sum of the two indications.
5. When flaws were combined due to proximity, the maximum depth of the combined indications was used.

In addition, the estimated crack growth until the next inspection was added for this evaluation. The shaded areas correspond to assumed indications. These results were determined using the proximity methodology presented in Reference 2-1.

2.1 References

2-1 BWR Core Shroud Inspection and Flaw Evaluation Guidelines, Prepared for the BWR Vessel and Internals Project Assessment Subcommittee, GENE-523-A113-0894, August 1994.

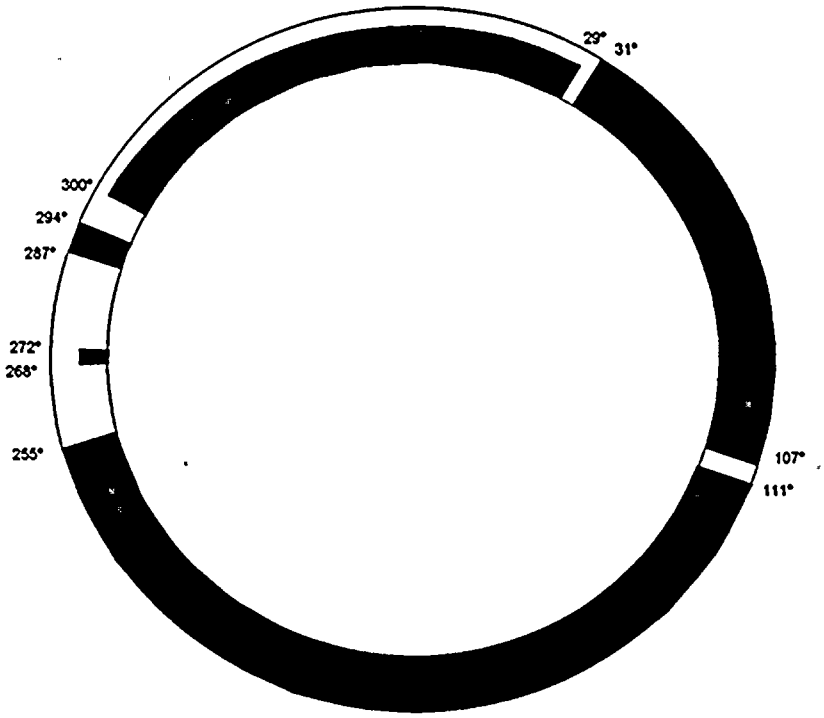

FIGURE 2-1 SCHEMATIC OF OYSTER CREEK INDICATIONS

3. COMPARISON BETWEEN NMP-1 AND OYSTER CREEK CORE SHROUDS

A comparison between the NMP-1 and Oyster Creek core shrouds is presented in this section. The intent is to demonstrate that any cracking in the NMP-1 shroud H4 weld is likely bounded by that observed in the Oyster Creek H4 weld. The evaluation considers water chemistry, fluence, on-line years, and material aspects.

3.1 Water Chemistry

For the first four cycle of hot operation, NMP-1 operated with relatively high primary water conductivity. As seen in Table 3-1 and Figure 3-1, the cyclic conductivity mean values exceeded 0.43 μS/cm. There was a dramatic conductivity improvement during the fifth fuel cycle where the conductivity decreased to less than 0.3 μS/cm. Since the fourth cycle, conductivity values have steadily improved and were excellent at less than 0.09 μS/cm during the last three operating cycles. Early steady state chloride levels ranged between 30 and 58 ppb. In addition to high early life steady state conductivity, there were a few documented water chemistry transients at NMP-1:

1. September 3, 1971 - NMP-1 conductivity reached 30 μS/cm at power due to high conductivity water in the condensate storage tank.
2. November 25, 1974 - NMP-1 conductivity reached 1.4 μS/cm at power due to a valving error during resin transfer. The pH dropped to 5.6 and 81 ppb chloride was identified in the water.
3. March 9, 1977 - 683 ppb chloride was identified in the water during shutdown.

Oyster Creek's early water chemistry was considerably more impure than NMP-1's. Oyster Creek was characterized by an average first seven cycle mean of 0.465 μS/cm. Only after fuel cycle ten, where data is again available, did the reactor water conductivity

improve. In fact, in 1991 Oyster Creek began operating on hydrogen water chemistry (HWC). The last three fuel cycle reactor water conductivity at Oyster Creek has been excellent.

Oyster Creek's early steady state chloride levels ranged over a slightly wider range than NMP-1, i.e., between 25 and 74 ppb. In addition to long term high early life steady state conductivity, there was a single documented water chemistry transient experienced at Oyster Creek (Reference 3-1).:

1. June 6, 1972 - 730 ppb chloride was identified in the water due to depleted reactor water clean-up system demineralizer.

Because of the high early life conductivity history, it is likely that intergranular stress corrosion cracking (IGSCC) initiation was accelerated in susceptible areas of the primary system, including the shroud. The effects of conductivity (sulfate) on crack initiation in uncreviced material is presented in Figure 3-2. It is clear that an increase in conductivity results in an acceleration in crack initiation as measured by the constant extension rate test (CERT). A similar type of initiation acceleration is observed for chloride ions.

The strong correlation between conductivity and IGSCC susceptibility in uncreviced sensitized stainless steel has also been examined in various other laboratory studies (Reference 3-2 through 3-4) and it is evident that a significant decrease in crack initiation time is expected with increased concentrations of certain deleterious anionic impurities, in particular chlorides and sulfates. For creviced BWR components, the strong correlation of SCC susceptibility with actual BWR plant water chemistry history has been Documented (Reference 3-5).

3.2 Shroud Evaluation

Following is a one-on-one comparison between the NMP-1 and Oyster Creek core shrouds:

- NMP-1's first five-cycle mean conductivity was 0.457 μS/cm compared to Oyster Creek at 0.526 μS/cm.
- NMP-1's total mean conductivity is 0.280 μS/cm compared to 0.316 μS/cm for Oyster Creek.
- NMP-1 is characterized by 15.5 on-line years compared to 15.7 for Oyster Creek.
- NMP-1 peak fast fluence is approximately 4.2×10^{20} n/cm^2. This compares against 6.6×10^{20} n/cm^2 for Oyster Creek.
- NMP-1's core shroud material and Oyster Creek core shroud material is essentially the same with both plants using the same heats of Type 304 stainless steel.
- Both NMP-1 and Oyster Creek shrouds were manufactured by P.F. Avery.

3.3 Shroud Comparison Conclusion

Based on the experience of shroud cracking in BWRs with relatively good water chemistry quality and at low fluence locations, independent of manufacturer, material of construction and relative age, cracking in NMP-1's H4 shroud weld cannot be ruled out. However, a on-on-one comparison between the operating history of NMP-1's and Oyster Creek strongly suggests that NMP-1's shroud is bounded by Oyster Creek's shroud condition. Although the material of shroud construction is identical in the two plants, the NMP-1 shroud corrosion considerations are favored by the lower first five cycle mean conductivity of the plant, lower total mean conductivity and lower fluence at the shroud.

3.4 References

3-1. B.H. Dillman et al, "Monitoring of Chemical Contaminants in BWRs, "EPRI NP-4134, July 1985.

3-2. Davis and M.E. Indig, "The Effect of Aqueous Impurities on the Stress Corrosion Cracking of Austenitic Stainless Steel in High Temperature Water," paper 128 presented at Corrosion 83, Anaheim, CA, NACE, April 1983.

3-3. Ljungberg. D. Cubiccioti and M. Tolle, "Effect of Impurities on the IGSCC of Stainless Steel in High Temperature Water," Corrosion, Vol. 44, No. 2, February 1988.

3-4. Ruther, W.K. Soppet and T.F. Kassner, "Effect of Temperature and Ionic Impurities at Very Low Concentrations on Stress Corrosion Cracking of Type 304 Stainless Steel," Corrosion, Vol. 44, No. 11, November 1988.

3-5. Brown and G.M. Gordon, "Effects of BWR Coolant Chemistry on the Propensity for IGSCC Initiation and Growth in Creviced Reactor Internals Components," paper presented at the Thrd Int. Symp. of Environmental Degradation of Materials in Nuclear Power Systems-Water Reactors, Transverse City, MI, August 1987, published in proceedings of the same, TMS-AIME, Warrendale, PA, 1988.

Table 3-1. Nine Mile Point-1 and Oyster Creek Water Chemistry History

Cycle	NMP-1 Cycle Mean Value Conduct. µS/cm	Oyster Cr Cycle Mean Value Conduct. µS/cm	NMP-1 Cl-ppb	OC Cl-ppb	NMP-1 SO_4=,ppb	OC SO_4=,ppb
1	0.432	0.426	30	40		
2	0.525	0.869	46	74		
3	0.591	0.329	58	27		
4	0.445	0.294	44	24		
5	0.291	0.714	33	37		
6	0.225	0.298	27	28		
7	0.181	0.324	26	25		
8	0.133		25			
9	0.087		18			
10	0.082	0.143	1	44	2	
11	0.084	0.144	1	2	3	
12		0.088		1		
13		0.09		1		
14		0.067		<1		2

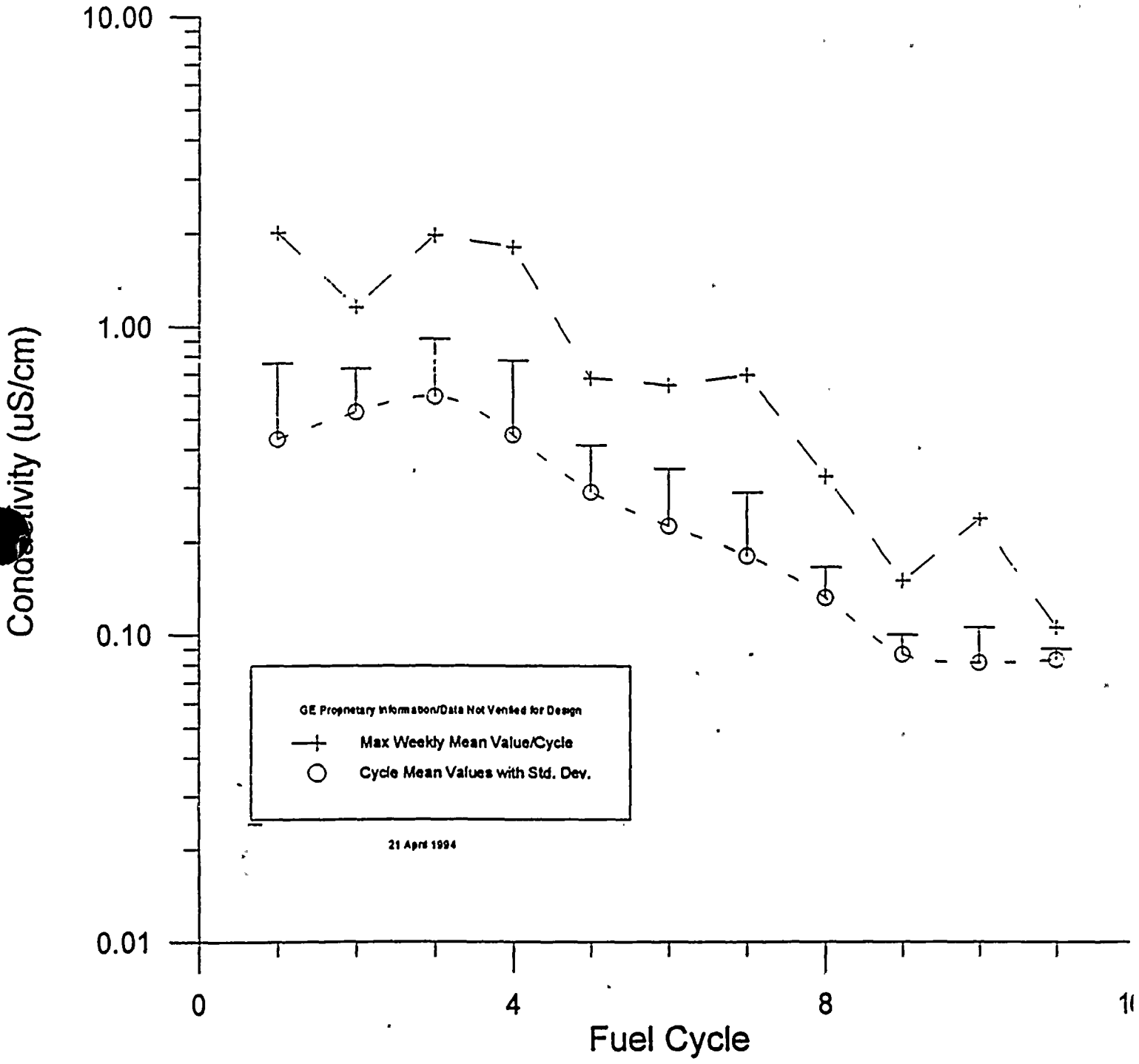

Figure 3-1 Nine Mile Point -1 Reactor Water Conductivity Mean Values

Figure 3-2. Effect of Sulfate on IGSCC Initiation Acceleration for FS Type 304

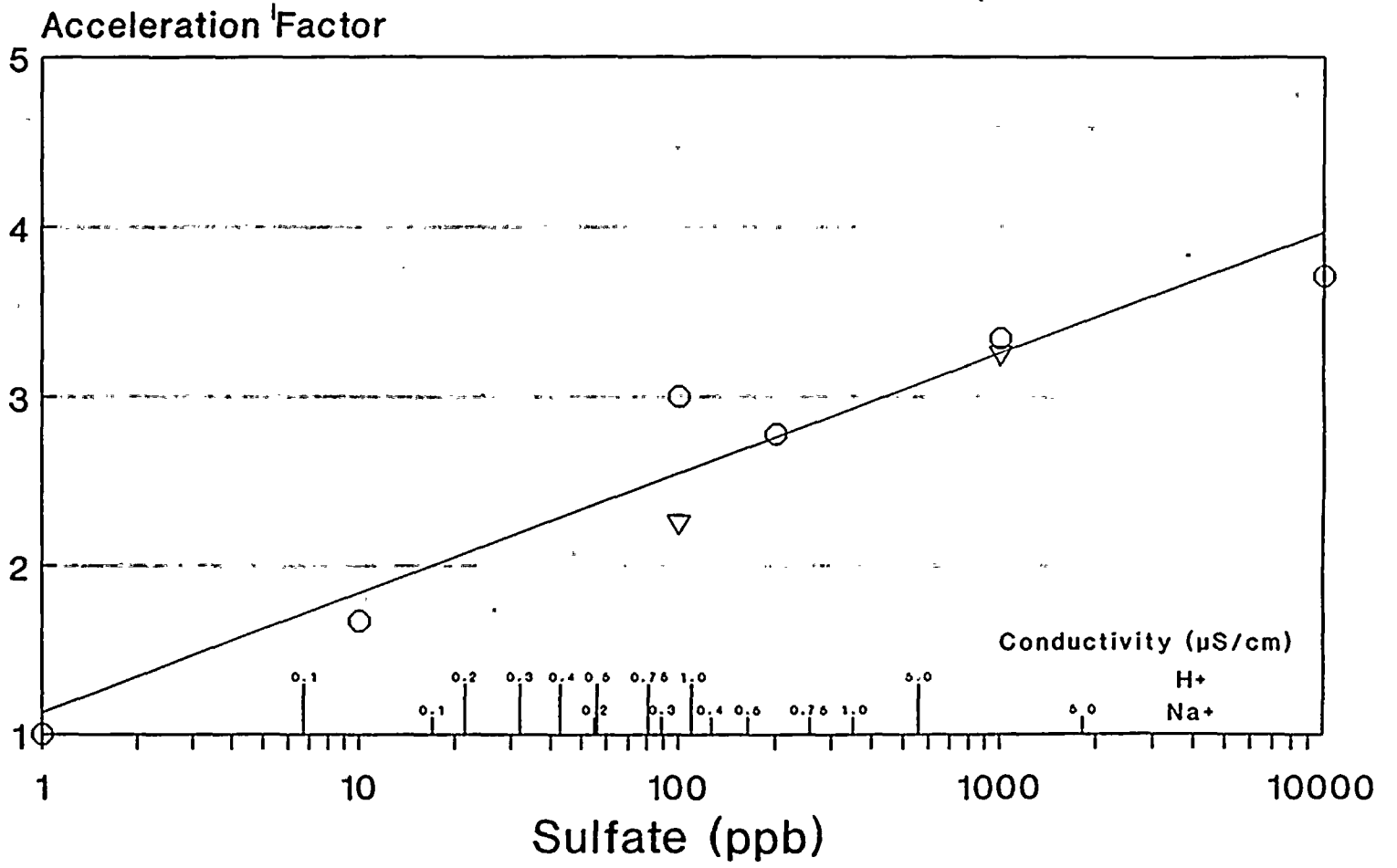

Crack initiation data based on CERT

SO4WCON

4. CRACK GROWTH ESTIMATE

The basis for the crack growth rate used in the screening criteria is provided in this section The NMP-1 shroud cylinders were fabricated from Type 304 stainless steel plate. Therefore, the weld heat-affected-zone (HAZ) is likely sensitized. The shroud is also subjected to neutron fluence during the reactor operation which further increases the effective degree of sensitization. The other side-effect of neutron fluence induced irradiation is the relaxation of weld residual stresses. The slip-dissolution model developed by GE quantitatively considers the degree of sensitization, the stress state and the water environment parameters, in predicting a stress corrosion cracking (SCC) growth rate. The crack growth rate predictions of this model have shown good correlation with laboratory and field measured values. This model was used to predict a crack growth rate and a conservative value was then selected.

The slip-dissolution model does not explicitly consider any contribution to crack growth due to new crack initiations. While new crack initiations during the next fuel cycle of operation can not be ruled out, considerable relaxation in weld residual stress magnitudes due to irradiation is likely to minimize crack initiation. This is supported by limited field evidence from an overseas plant where the same cracked region of the shroud was examined over three refueling cycles following the discovery of first incidence of cracking. The subsequent examinations showed some growth of the existing crack, but did not show evidence of new initiations. Even if any new initiations do occur, it is likely that only shallow cracking will occur during one cycle of operation.

4.1 Slip-Dissolution Model

Figure 4-1 schematically shows the GE slip-dissolution film-rupture model (Reference 4-1) for crack propagation. The crack propagation rate V_t is defined as a function of two constants (A and n) and the crack tip strain rate, $\dot{\varepsilon}_{ct}$.

$$V_t = A\dot{\varepsilon}_{ct}^{n} \qquad (4\text{-}1)$$

where: $\dot{\varepsilon}_{ct} = CK^4$ (for constant load)

$A = 7.8\times10^{-3} n^{3.5}$ (from Reference 4-2)

$n = \{ e^{f(\kappa)} / (e^{f(\kappa)} + e^{f(\varphi)c})\} f(EPR)$ (from Reference 4-2)

The constants are dependent on material and environmental conditions. The crack tip strain rate is formulated in terms of stress, loading frequency, etc. When a radiation field, such as the case for the shroud, is present, there is additional interaction between the gamma field and the fundamental parameters which affect intergranular stress corrosion cracking (IGSCC) of Type 304 stainless steel (see Figures 4-2 and 4-3).

The increase in sensitization (i.e., Electrochemical Potentiokinematic Reactivation, EPR) and the changes in the value of constant A and n as a function of neutron fluence (>1MeV) is given as the following:

$$EPR = EPR_0 + 3.36 \times 10^{-24} (\text{fluence})^{1.17} \quad (4\text{-}2)$$

where, EPR is in units of C/cm^2, fluence is in units of n/cm^2 and the calculated value of EPR has an upper limit of 30.

The constant C is defined as the following:

$$\text{for fluence} \leq 1.4 \times 10^{19}\ n/cm^2\text{: } C = 4.1 \times 10^{-14} \quad (4\text{-}3a)$$

$$\text{for fluence} > 1.4 \times 10^{19}\ n/cm^2 \text{ but } \leq 3 \times 10^{21}\ n/cm^2\text{:}, \quad C = 1.14 \times 10^{-13} \ln(\text{fluence}) - 4.98 \times 10^{-12} \quad (4\text{-}3b)$$

$$\text{for fluence} \leq 3.0 \times 10^{21}\ n/cm^2\text{: } C = 6.59 \times 10^{-13} \quad (4\text{-}3c)$$

The variable K is the stress intensity via linear elastic fracture mechanics and is to be used with the above expressions in the units of $MPa\sqrt{m}$.

4.2 Calculation of Parameters

The parameters needed for the crack growth calculation by the GE model are: stress state and stress intensity factor, effective EPR, water conductivity, and electro-chemical corrosion potential (ECP).

The stress state relevant to IGSCC growth rate is the steady state stress which consists of weld residual stress and the steady applied stress. Figure 4-4 shows observed through-wall weld residual stress distribution for large diameter pipes. The residual stress is tensile

at both the inside and outside surfaces and compressive in the middle. This type of distribution (characterized by a cosine function) is a conservative representation for welds in large diameter pipes and plates (see Reference 4-3). The maximum stress at the surface was nominally assumed as 35 ksi. The steady applied stress on the shroud is due to core differential pressure and its magnitude is small compared to the weld residual stress magnitude. Figure 4-5 shows the assumed total stress profile used in the evaluation. Figure 4-6 shows the calculated values of stress intensity factor (K) assuming a 360° circumferential crack. It is seen that the calculated value of K reaches a maximum of approx. 25 ksi$\sqrt{in}$. The average value of K was estimated as 20 ksi$\sqrt{in}$ and was used in the crack growth rate calculations.

The weld residual stress magnitude is expected to decrease as a result of relaxation produced by irradiation-induced creep. Figure 4-7 shows the stress relaxation behavior of Type 304 stainless steel due to irradiation at 550° F. Since most of the steady stress in the shroud comes from the weld residual stress, it was assumed that the K values shown in Figure 4-6 decrease in the same proportion as indicated by the stress relaxation behavior of Figure 4-7.

The second parameter needed in the evaluation is the EPR. In the model, the initial EPR value is assumed as 15 for the weld sensitized condition. Using Equation (4-2), the predicted increase in EPR value as a function of fluence is shown in Figure 4-8.

The third parameter used in the GE predictive model is the water conductivity. A water conductivity of 0.1 $\mu S/cm$ was used in this calculation which is a reasonable value for many plants. The reactor water conductivity at NMP-1 is excellent (approx. 0.084 $\mu S/cm$). This has a significant impact on the predicted crack growth rate by the GE model as seen in Figure 4-9, as shown for a domestic BWR/4. To demonstrate that the GE model conservatively reflects the effect of conductivity, Figure 4-10 shows a comparison of the GE model predictions with the measured crack growth rates in the crack advance verification system (CAVS) units installed at several BWRs. The comparison with CAVS data in Figure A-10 also demonstrates the conservative nature of crack growth predictions by the GE model.

The last parameter needed in the GE prediction model is the ECP. Figure 4-11 shows the measured values of ECP at two locations in the core. The ECP values at zero H_2 injection are relevant in Figure A-11 for no hydrogen injection. It is seen that the ECP

values at zero H_2 injection rate range from 150 mV to 225 mV. Therefore, a value of 200 mV was used in the calculation.

4.3 Crack Growth Prediction

Based on the discussion in the preceding section, the crack growth rate calculations were conducted as a function of fluence assuming the following values of parameters:

Initial K	= 20 ksi$\sqrt{in}$
EPR_0	= 15 C/cm^2
Cond.	= 0.1 μS/cm
ECP	= 200 mV

Figure 4-12 shows the predicted crack growth rate as a function of fluence. It is seen that the predicted crack growth rate initially increases with the fluence value but decreases later as a result of significant reduction in the K value due to irradiation induced stress relaxation. The crack growth rate peaks at 4.5×10^{-5} in/hr at a fluence of 1×10^{20} n/cm^2. Thus, a bounding value of 5×10^{-5} in/hr can be conservatively used in the structural integrity evaluation for the shroud.

The actual recent water conductivity for NMP-1 is 0.084 μS/cm. A NMP-1 plant specific calculation was also performed using the NMP-1 water conductivity and current fluence at the H4 weld. Results of this calculation showed that the NMP-1 crack growth rate was 2.6×10^{-5} in/hr. For purposes of this evaluation, a conservative crack growth rate of 5×10^{-5} in/hr is used.

This bounding crack growth rate is quite conservative as can be shown in Figure A-13 from NUREG-0313, Rev. 2. It is seen that the crack growth rate of 5×10^{-5} in/hr at 20 ksi$\sqrt{in}$ is considerably higher than what would be predicted by using the NRC curve. This further demonstrates the conservatism inherent in the assumed bounding value of crack growth rate.

4.4 Conclusion

A crack growth rate calculation using the GE predictive model was conducted considering the steady state stress, EPR, conductivity and ECP values for a typical shroud. The evaluation accounted for the effects of irradiation induced stress relaxation and the increase in effective EPR. The evaluation showed that a bounding crack growth rate of 5×10^{-5} in/hr may be used in the structural integrity evaluation of the NMP-1 shroud.

4.5 Reference

4-1 F.P. Ford et al, "Prediction and Control of Stress Corrosion Cracking in the Sensitized Stainless Steel/Water System," paper 352 presented at Corrosion 85, Boston, MA, NACE, March 1985.

4-2 F. P. Ford, D. F. Taylor, P. L. Andresen & R. G. Ballinger, "Environmentally Controlled Cracking of Stainless Steel and Low Alloy Steels in LWR Environments," 1987, (EPRI Report NP50064M, Contract RP2006-6).

4-3 ASME Section XI Task Group on Reactor Vessel Integrity Requirements, "White Paper on Reactor Vessel Integrity Requirements for Level A and B Conditions," EPRI, Palo Alto, CA, January 1993, (EPRI Report TR-100251, Project 2975-13).

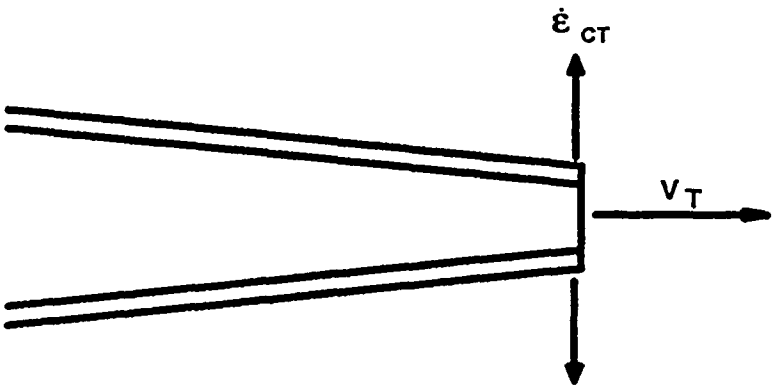

$$V_T = A\,\dot{\varepsilon}_{CT}^{n}$$

Where:

- V_T = crack propagation rate
- A, n = constants, dependent on material and environmental conditions,
- $\dot{\varepsilon}_{CT}$ = crack-tip strain rate, formulated in terms of stress, loading frequency, etc.

Figure 4-1: The GE PLEDGE Slip Dissolution - Film Rupture Model of Crack Propagation

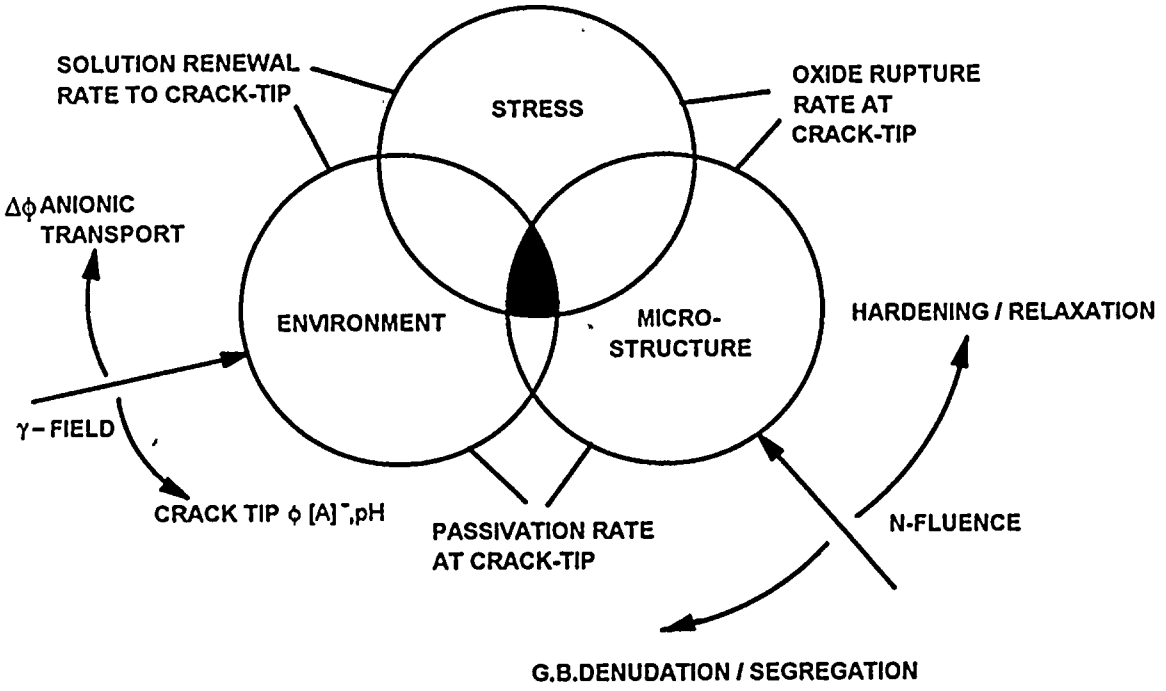

Figure 4-2: Effects of Fast Fluence, Flux & Gamma Field on Parameters Affecting IGSCC of Type 304 Stainless Steel

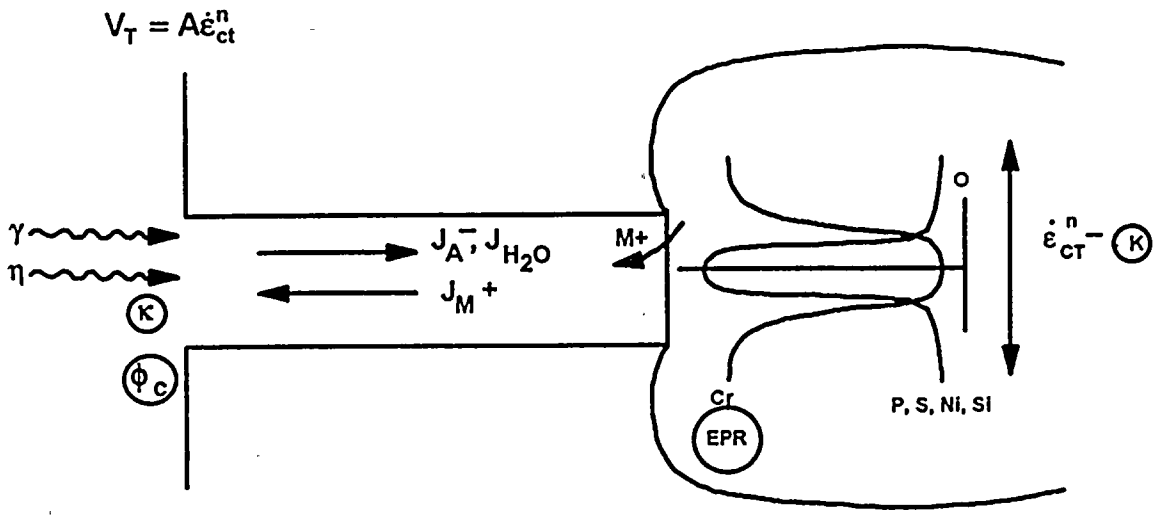

$$V_T = A\dot{\varepsilon}_{ct}^n$$

$$n = \{ e\, f(\kappa) / (e^{f(\kappa)} + e\, f(\varphi)c) \}\, f(EPR)$$

Figure 4-3: Parameters of Fundamental Importance to Slip Dissolution Mechanism of IGSCC in Sensitized Austenitic Stainless Steel

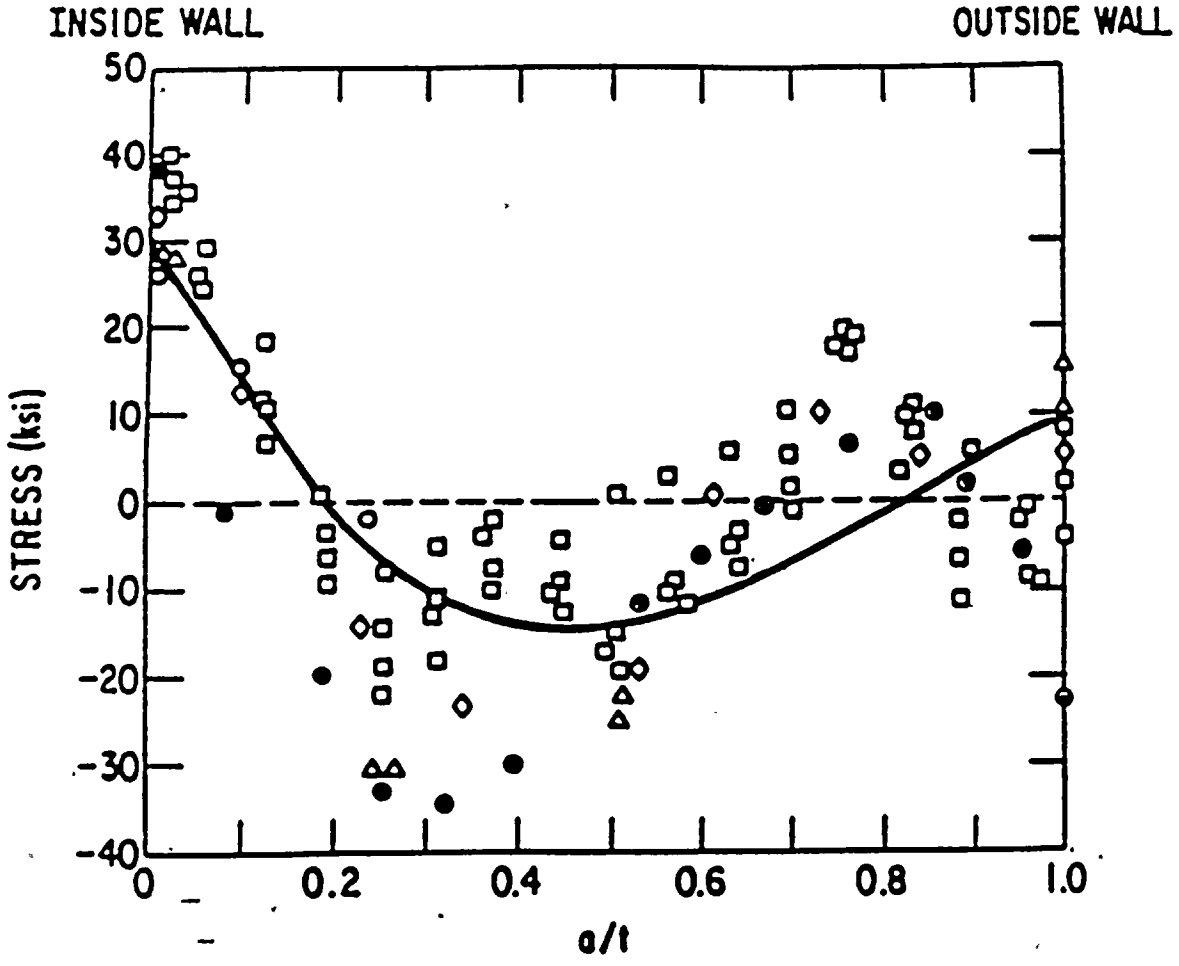

Figure 4-4: Through-wall Longitudinal Residual Stress Data Adjacent to Welds in 12 to 28 inch Diameter Stainless Steel Piping

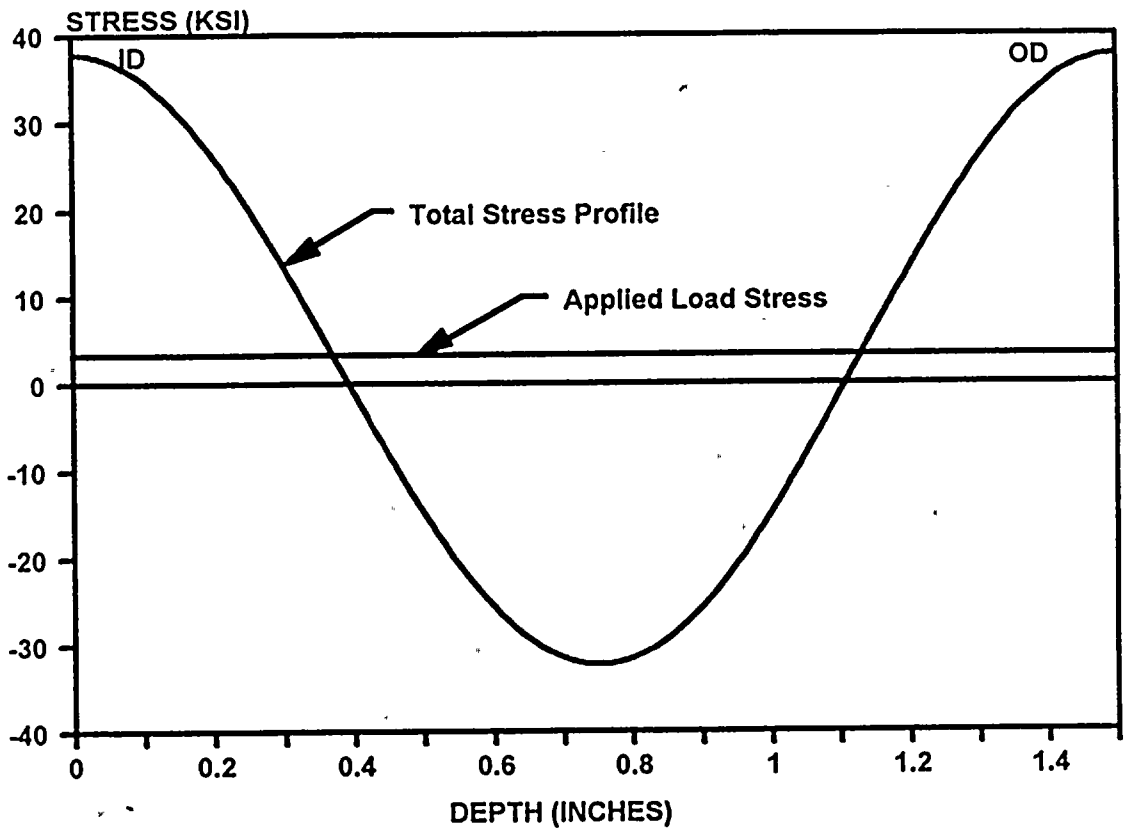

Figure 4-5: Conservative Representation of the Shroud Total Through-wall Stress Profile

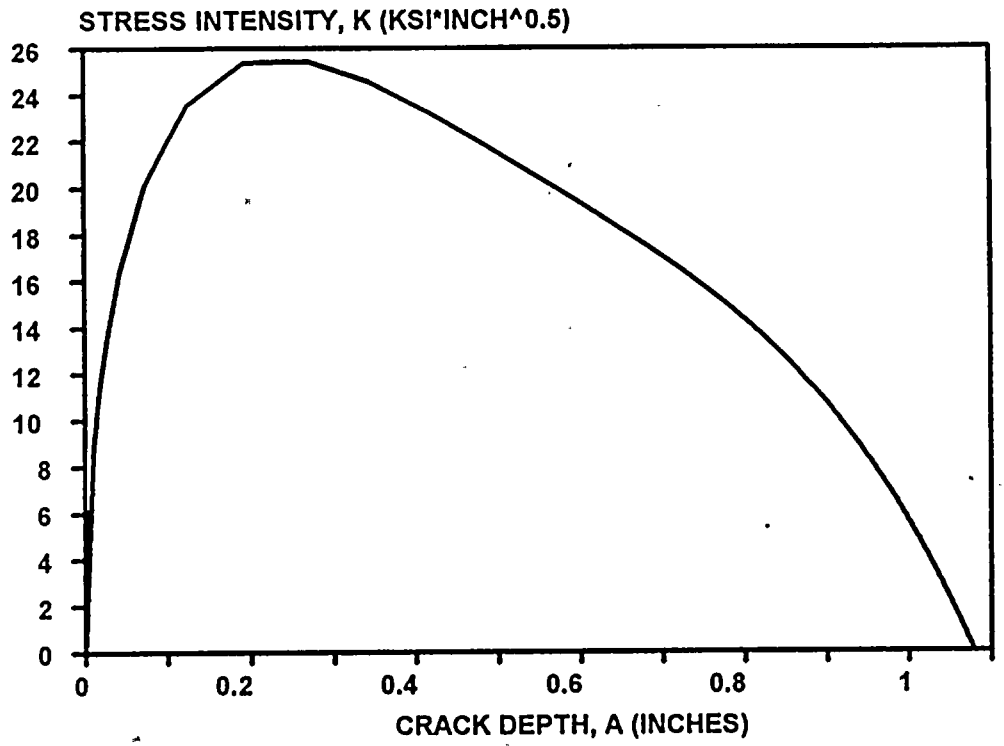

Figure 4-6: Shroud Through-wall Stress Intensity Factor

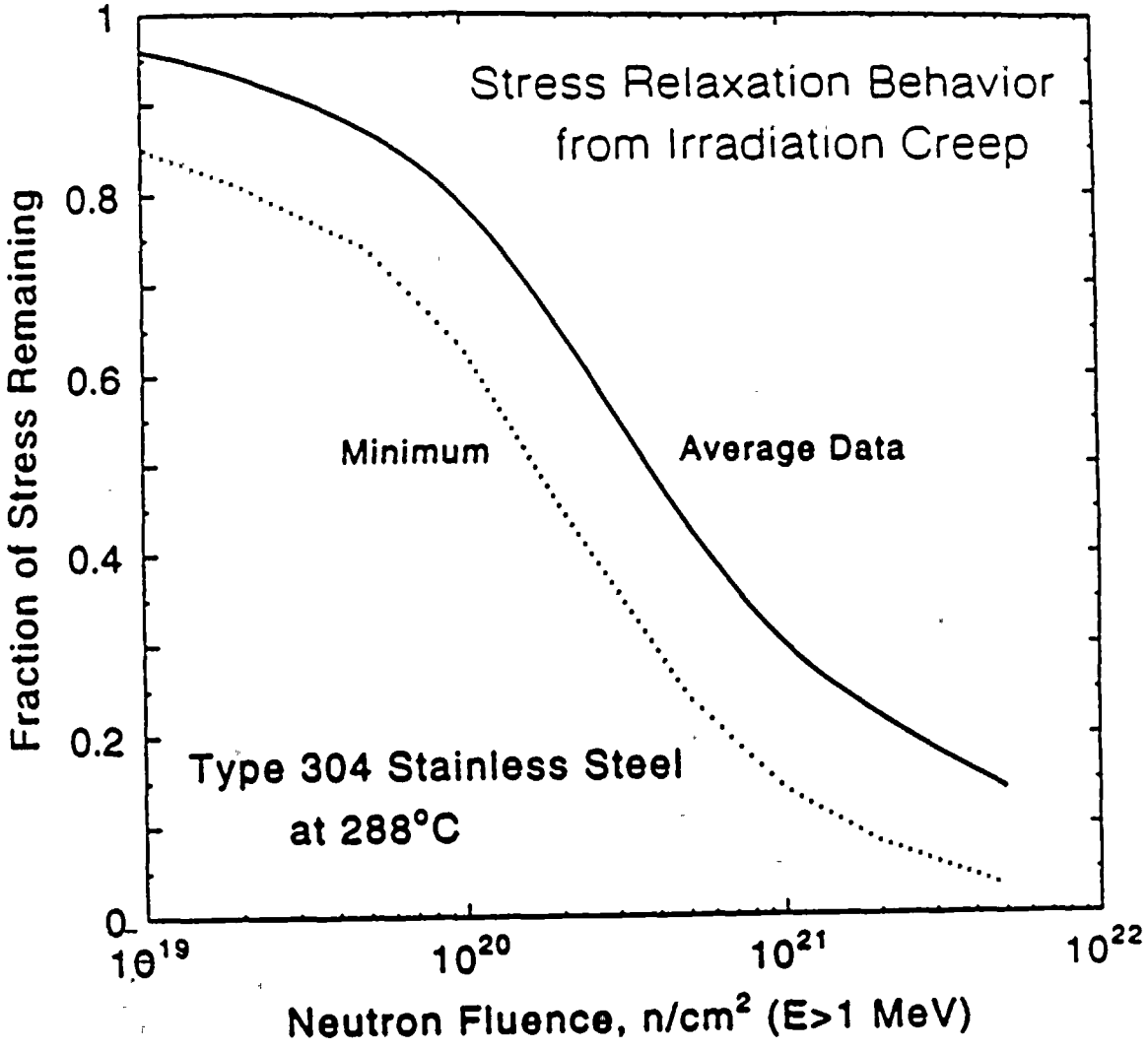

Figure 4-7: Stress Relaxation Behavior of Type 304 Stainless Steel Due to Irradiation at 288°C

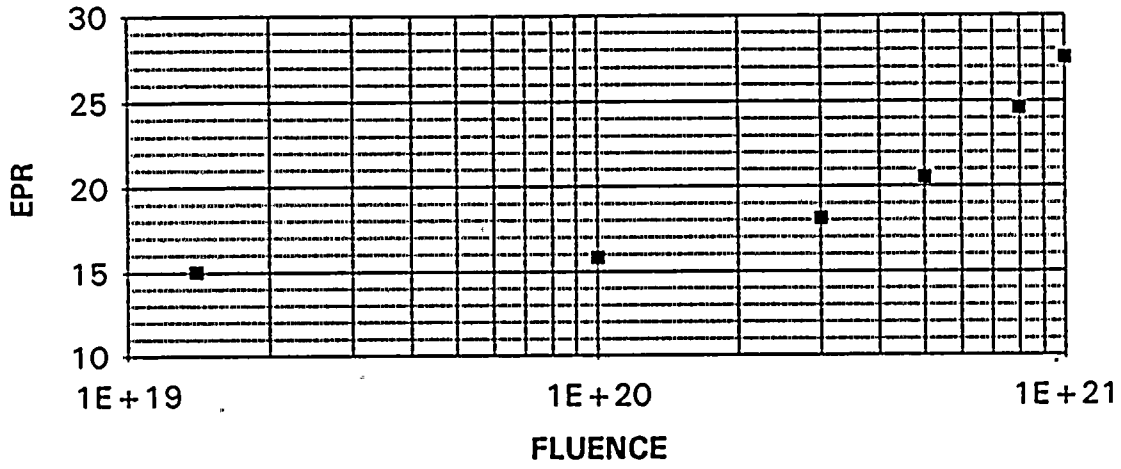

Figure 4-8: EPR Versus Neutron Fluence

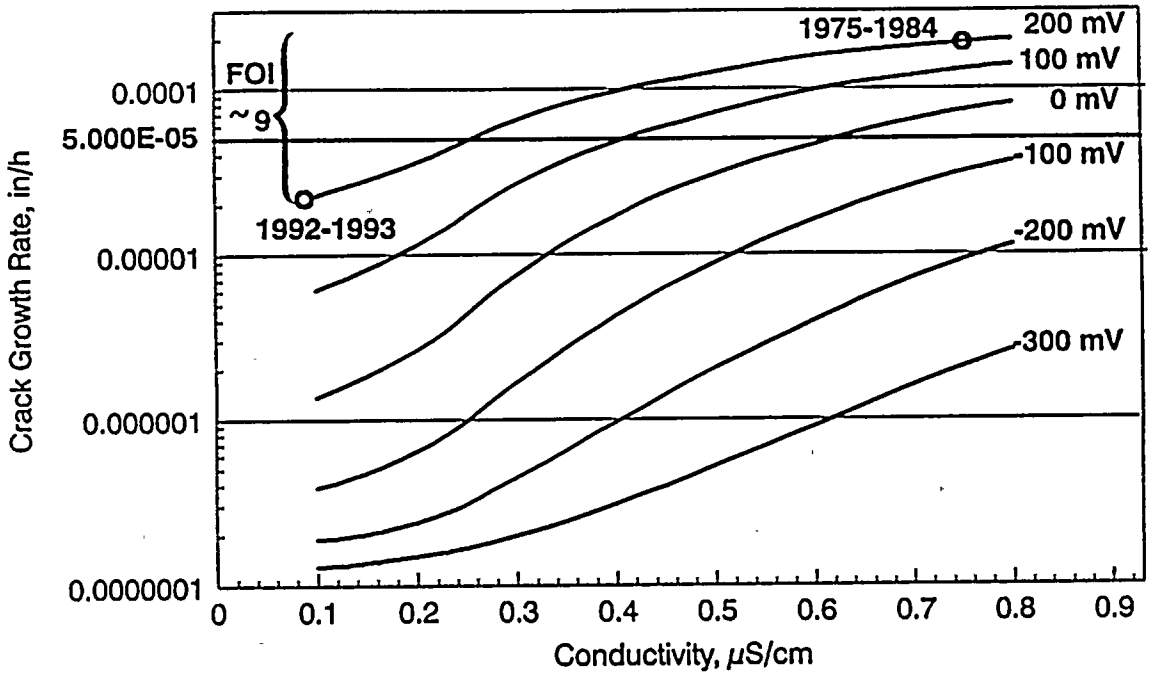

PLEDGE: 20 ksi$\sqrt{in}$, 15 C/cm^2

Figure 4-9: GENE PLEDGE Model Prediction for a BWR-4 (Sensitized Type 304 Crack Growth Rate)

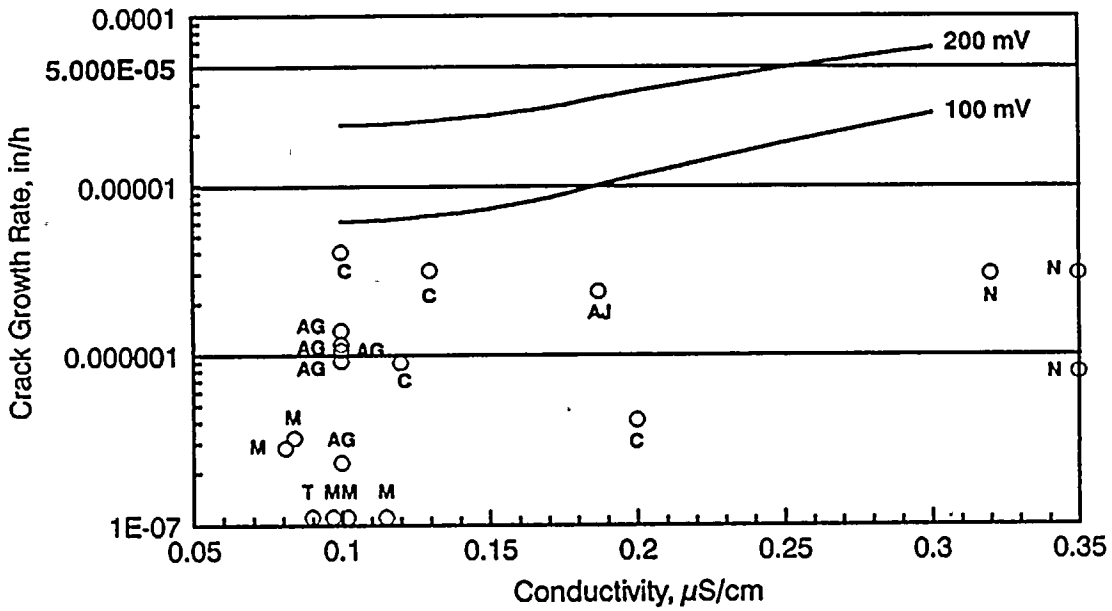

PLEDGE: 20 ksi$\sqrt{in}$, 15 C/cm^2

CAV: 20-25 ksi$\sqrt{in}$, 13 C/cm^2, 100-160 mV

Figure 4-10: Effect of Conductivity on Sensitized Type 304 Crack Growth Rate

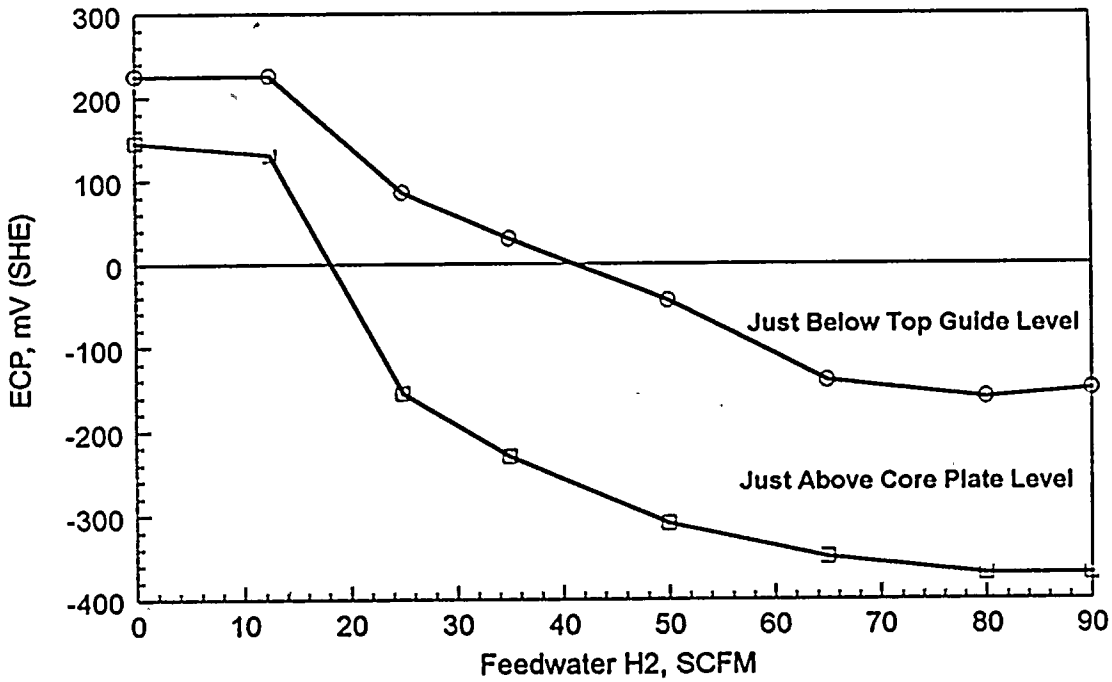

Figure 4-11: In-Core Bypass ECP versus Feedwater Hydrogen for BWR-4

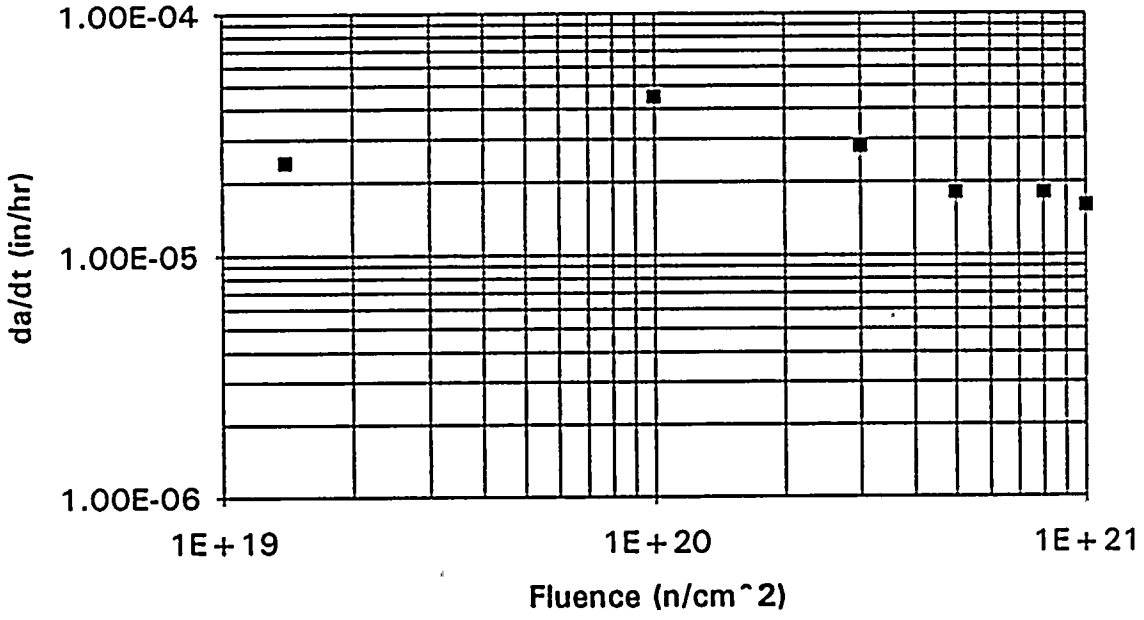

– Stress Intensity = 20 ksi$\sqrt{in}$, Initial EPR = 15 C/cm^2

Figure 4-12: Growth Rate versus Fluence

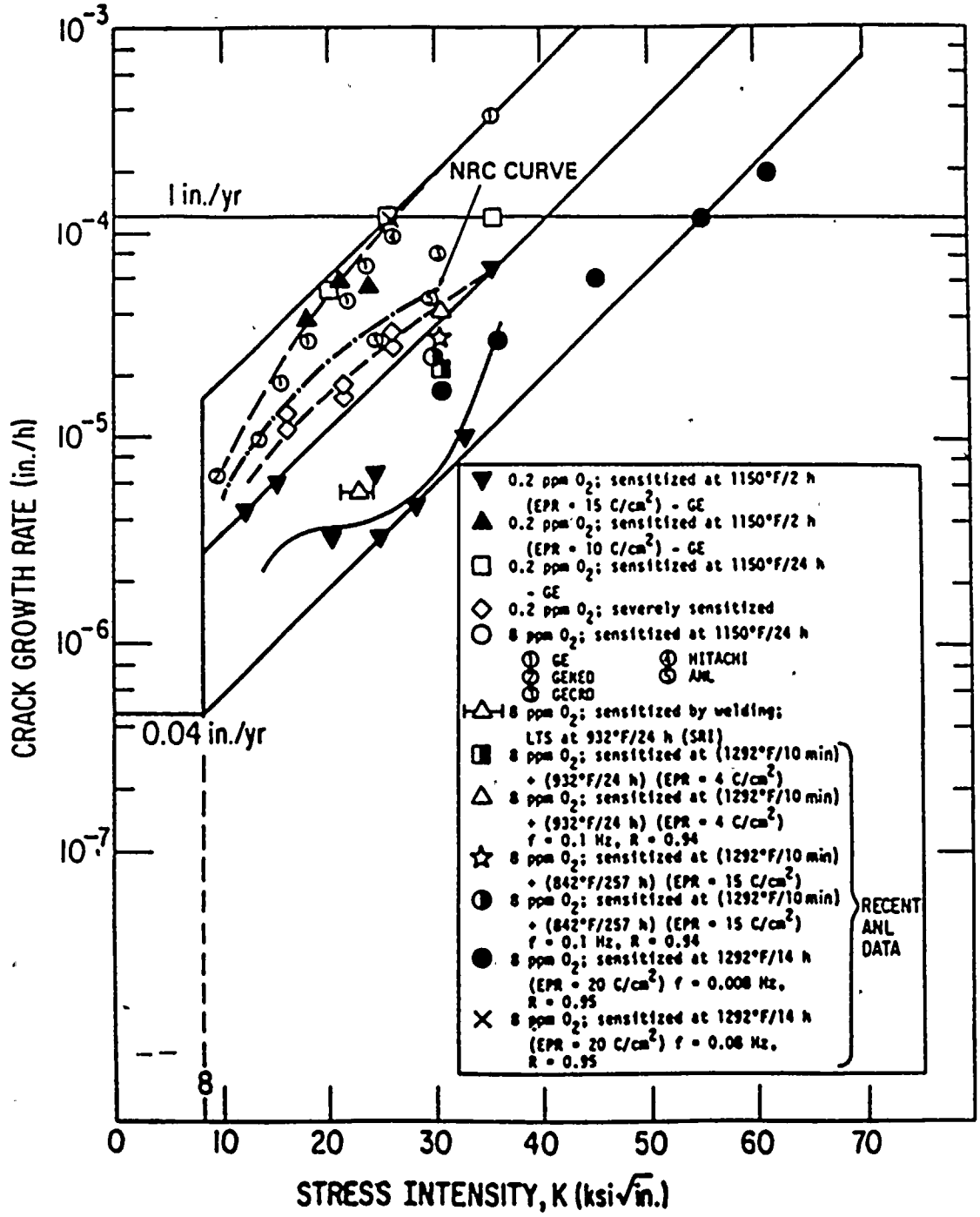

Figure 4-13: NUREG-0313 Crack Growth Rate Data

5. FLAW EVALUATION

This section provides the methodology and evaluation of the observed indications in the Oyster Creek H4 weld. This method incorporates the conservative assumption that the areas other than the inspected ligament lengths are assumed to be cracked through wall, and considers proximity rules.

A brief description of the techniques is first provided followed by a detailed description of the evaluation.

5.1 Limit Load Method

Figure 5-1 shows a schematic representative plan view of an asymmetric distributed uncracked ligament. It is assumed that there are 1,2,...i,.... n ligament lengths and that the i^{th} length is of thickness 't_i' and extends from an azimuth of θ_{i1} to θ_{i2}. The ligament length 'l_i' of the ith ligament is related to azimuth angles θ_{i1} and θ_{i2} by the following relationship:

$$l_i = (D/2) \bullet (\theta_{i1}-\theta_{i2}) \qquad (5\text{-}1)$$

where, D is the diameter of the shroud. The calculation of moment 'M' that this ligament configuration can resist, is somewhat complicated since it is not a priori clear as to which azimuthal orientation of the neutral/central axis would produce the least value of bending moment, 'M'. Therefore, the value of 'M' is calculated for various orientations of the central axis from 0° to 360°. This calculation is performed in two steps:

(1) In this step, a central axis orientation, α, is first selected. The location of the neutral axis (which is parallel to the central axis) at a distance δ from the central axis is determined using the following (see Figure 5-1):

$$\int_{-(\pi-\alpha+\beta)}^{\alpha+\beta} Rt(\theta)d\theta - \int_{\alpha+\beta}^{-(\pi-\alpha+\beta)} Rt(\theta)d\theta = (\sigma_m/\sigma_f)(2\pi Rt_n) \qquad (5\text{-}2)$$

where, α = Assumed azimuth angle of the central axis

β = Angle of the neutral axis with respect to central axis, or $\sin^{-1}(\delta/R)$

δ	=	Distance between the central axis and the neutral axis
R	=	Mean radius of the shroud
$t(\theta)$	=	t_i (thickness of the ith ligament), if angle θ is such that $\theta_{i1} < \theta < \theta_{i2}$, or 0 otherwise.
t_n	=	Nominal thickness of shroud
σ_m	=	Membrane stress
σ_f	=	Material flow stress = $3S_m$

Thus, this step helps define the location of the neutral axis when the central axis is assumed to be at an azimuth angle of α.

(2) Once the location of the neutral axis relative to the central axis is determined, the moment, M_α, is then obtained by integrating the bending moment contributions from individual ligament lengths. The mathematical expression used is the following:

$$M_\alpha = \int_0^{2\pi} \sigma_f R^2 A\, t(\theta) \sin(\alpha - \theta)\, d\theta \qquad (5\text{-}3)$$

where, A = 1.0, if $-(\pi-\alpha+\beta) < \theta < \alpha+\beta$, or
-1.0, if $\alpha+\beta < \theta < -(\pi-\alpha+\beta)$

The orientation 'α' that produces the least value of M is called 'α,min' and defines the axis capable of resisting the limiting moment. Whether the specified set of uncracked ligament lengths provides the required structural margin is verified by the following:

$$-M_{\alpha,min}/Z + P_m \geq SF(P_m+P_b) \qquad (5\text{-}4)$$

where,

Z	=	Section modulus of the shroud based on uncracked cross section
P_m	=	Applied membrane stress
P_b	=	Applied bending stress
SF	=	Safety factor

5.2 Evaluation of Part-Through Wall Cracks

If it is not possible obtain the required safety factors assuming through-wall indications, then evaluation of a combination of uncracked ligaments and part through-wall cracks may be required to assess structural margins. For this case, the angular location of the uncracked ligaments, and the depth of the flaws, must be determined. Proximity rules are used to determine effective flaw length. The depth determination must also include any uncertainty associated with the NDE method used. Allowances for crack growth are also factored in, including effects on both length of uncracked ligaments, and depth of flawed portions of the area examined. This information can then be analyzed in accordance with previously outlined methods.

The maximum observed depth sizing error to date has been 7.6 mm. Based on this, the uncertainty assigned to depth measurements is 7.6 mm, until better information can be obtained.

It may be possible to conservatively simplify the above approach by assuming a flaw of 360° at the maximum observed depth, a. The depth 'a' should include any uncertainty associated with the NDE method used.

The required minimum 360° ligament at a circumferential weld can be determined by iteratively calculating the allowable crack depth, 'd' using the following equations (Reference 5-1):

$$\beta = \{\pi(1-d/t_n-P_m/\sigma_f)\}/(2-d/t_n) \quad (5\text{-}5)$$

$$P_b' = (2\sigma_f/\pi)(2-d/t_n)\sin\beta \quad (5\text{-}6)$$

$$(P_m+P_b)SF = P_b' + P_m$$

where,

- P_m = Primary membrane stress at the subject weld
- P_b = Primary bending stress at the subject weld
- d = Allowable crack depth
- t_n = Shroud wall thickness (away from a fillet weld)
- SF = Safety factor appropriate for the operating condition being evaluated
- σ_f = Material flow stress (= $3S_m$)

It should be noted that the stresses, P_m and P_b, are calculated using the nominal shroud thickness. The current crack depth 'a' is acceptable if the projected crack depth, after accounting for crack growth until the next inspection, is less than the allowable crack depth 'd'. This criteria is given by the following equation:

$$(a + CG) \quad < \quad d \qquad (5\text{-}7)$$

where, CG is the projected crack growth until the next inspection.

5.3 Safety Factors

Safety factors of 2.8 for operational conditions and 1.4 for faulted conditions were used in the evaluation of circumferential welds. These safety factor values are consistent with Section XI values.

5.4 Application of Flaw Evaluation Methodology to NMP-1 Shroud

The application of the flaw evaluation methodology described earlier is presented in this section. Crack growth assuming a crack growth rate of $5x10^{-5}$ in/hr was added to the assumed indications.

5.4.1 Limit Load

For limit load, the flaw distribution pattern in Section 2.0 was used. This flaw distribution pattern was a result of applying the proximity criteria given in Reference 2-1. A computer program was used which uses the Reference 2-1 methodology. Results of this evaluation showed safety factors in excess of those required. The resulting safety factors were:

Condition	Calculated	Required
Normal and Upset	6.5	2.8
Emergency and Faulted	3.5	1.4

These results illustrate that due to the relatively low loads, the shroud is very flaw tolerant.

5.4.2 LEFM

The LEFM calculation is provided even though the results of this calculation may not be meaningful due to the fluence at the NMP-1 H4 weld location. The current fluence is just above $3x10^{20}$ n/cm^2. The fracture toughness used to determine the critical flaw size corresponds to material with a fluence of $8x10^{20}$ n/cm^2.

Based on the Oyster Creek flaw results, a conservative combination of the indications was considered for the LEFM calculation. Using this conservative combination, a safety factor of 1.83 was obtained. This compares against the required 1.4 for faulted conditions.

5.5 References

5-1 S. Ranganath and H.S. Mehta, "Engineering Methods for the Assessment of Ductile Fracture Margin in Nuclear Power Plant Piping," ASTM STP 803 (1983).

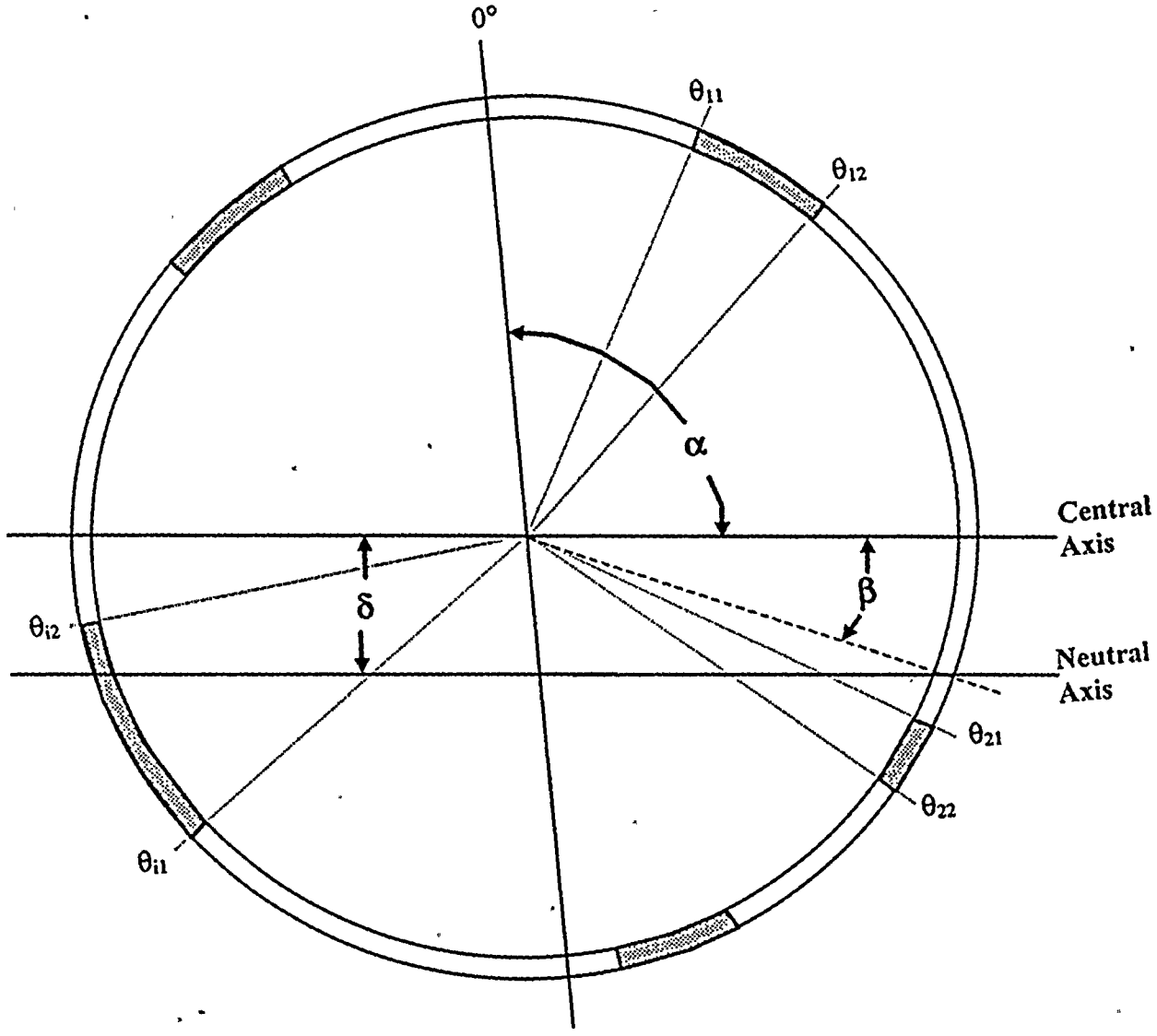

Figure 5-1 Schematic of Non-Symmetric Ligament Distribution

6. CONCLUSIONS

An evaluation of the NMP-1 core shroud has been performed. The objective of the evaluation was to demonstrate that continued operation of NMP-1 was justified on a structural basis by applying the Oyster Creek inspection results to NMP-1. It was concluded that based on a one-to-one comparison between NMP-1 and Oyster Creek, the indications in the Oyster Creek shroud will likely bound those in the NMP-1 shroud. Even with this conservative assumption, it was determined that the safety factor present in the NMP-1 core shroud (using Oyster Creek indications) exceeded the required safety factors until at least February of 1995.

Thus, it was concluded that continued operation of the NMP-1 plant is justified based on structural evaluation of the core shroud.

ATTACHMENT 2

NINE MILE POINT UNIT 1
DOCKET NO. 50-220
LICENSE NO. DPR-63

GENERIC LETTER 94-03
SUPPLEMENTAL INFORMATION

"FRACTURE MECHANICS ASSESSMENT OF THE NINE MILE POINT UNIT 1 SHROUD H4 WELD"

REPORT MPM-109439
MPM RESEARCH & CONSULTING
OCTOBER 1994